# Experimental characterization of the optical klystron effect to measure the intrinsic energy spread of high-brightness electron beams

Eduard Prat,[1,*] Christoph Kittel,[1,2] Marco Calvi,[1] Paolo Craievich,[1] Philipp Dijkstal,[1] Sven Reiche,[1] Thomas Schietinger,[1] and Guanglei Wang[1]

[1]*Paul Scherrer Institut, CH-5232 Villigen PSI, Switzerland*
[2]*University of Malta, MSD2080 Msida, Malta*

(Received 20 December 2023; accepted 9 February 2024; published 1 March 2024)

The intrinsic energy spread of electron beams needs to be measured to characterize and optimize high-brightness electron beam sources such as those driving x-ray free-electron lasers (FELs). We demonstrate the use of the optical klystron effect as a precise and high-resolution method to measure the electron beam energy spread. The optical klystron setup consists of undulator modules and magnetic chicanes placed between them. The energy spread is found by measuring the radiation power produced in the undulators as a function of the chicanes' strengths. High resolution and simplicity are the advantages of this approach, in contrast to the standard method, which measures the longitudinal phase space of the electron beam with a transverse deflector. The demonstration was performed at Athos, the soft x-ray FEL beamline of SwissFEL, for which we measured energy spreads below 1 MeV at a central beam energy of 3.4 GeV. We have verified the consistency of the method for different parameters (radiation wavelengths, undulator polarization configurations, and electron bunch durations) and we have benchmarked it against the standard measurement approach using a transverse deflector. Our results confirm the optical klystron as a valid approach to measure the electron beam energy spread. The method can be especially useful to reconstruct low energy spread values, where the conventional approach may be resolution limited, such as in ultra high-brightness radiofrequency photoinjectors or plasma sources, or when transverse deflectors are not available.

DOI: 10.1103/PhysRevAccelBeams.27.030701

## I. INTRODUCTION

High-brightness or -brilliance electron beams are fundamental for cutting-edge scientific applications such as x-ray free-electron lasers (FELs) [1–3], electron diffraction [4,5], and radiation sources based on inverse Compton scattering [6,7]. Radio-frequency (rf) photoinjectors [8,9] are the standard technological choice to generate high-brightness electron beams. There are extensive global efforts to enhance the brightness of rf photoinjectors [10–13], as well as to elaborate potentially brighter technologies such as plasma sources [14–16].

The six-dimensional electron beam brightness or brilliance can be written as [17]:

$$B = \frac{Q}{\varepsilon_{n,x}\varepsilon_{n,y}\varepsilon_{n,s}} \approx \frac{I}{\varepsilon_{n,x}\varepsilon_{n,y}c\sigma_E}, \tag{1}$$

where $Q$ is the electron bunch charge, $\varepsilon_{n,x}$ and $\varepsilon_{n,y}$ are the horizontal and vertical normalized emittances, $\varepsilon_{n,s}$ is the longitudinal emittance, $I$ is the electron beam peak current, $c$ is the speed of light, and $\sigma_E$ is the intrinsic or uncorrelated energy spread of the electron beam. From this moment, we will refer to the intrinsic or uncorrelated energy spread simply as energy spread. In the above expression, we take the longitudinal emittance as the product of the longitudinal beam size $\sigma_s$ and the energy spread, assuming no significant impact of the energy chirp. We also consider $I = Q/\sigma_t$, with $\sigma_t \approx \sigma_s/c$. Smaller transverse emittances, smaller energy spread, or higher current enhance the brightness of electron beam sources. The energy spread should be measured and optimized to maximize the brightness of the electron beam source.

In this report, we will focus on the high-brightness electron sources driving x-ray FELs, for which the electron beam energy spread is a fundamental parameter. A lower energy spread is associated with a better FEL performance in terms of saturation power and length, with the possibility of compressing the electron beams more strongly and therefore achieving shorter pulses, and with improving the efficiency of externally seeded FELs [18,19] in terms of required external laser power and achievable final

*eduard.prat@psi.ch

wavelength. Indeed, precise knowledge of the energy spread of the electron beam is fundamental to setting up externally seeded FELs.

A typical x-ray FEL facility consists of an rf photoinjector, where the high-brightness electron beam is produced, a linac to accelerate and compress the electron beam, and an undulator, where the x-ray radiation is generated. rf photoinjectors generate electron beams with energies of around 10 MeV, peak currents of around 20 A, corresponding, for typical bunch charges of 200 pC, to an rms bunch duration of a few picoseconds, and design energy spread values at the keV level or below. In the linac section, the electron beam is accelerated to energies of several GeV and compressed to peak currents of a few kA, or electron bunch durations of a few tens of femtoseconds. The electron beam is typically compressed in two or three stages. The electron beam energy is usually a few hundreds of MeV in the first compression stage and reaches the GeV level in the final stage. Assuming no coupling between the transverse and longitudinal planes, the longitudinal emittance is at best preserved according to Liouville's theorem. Therefore, the energy spread will increase up to the MeV level in the undulator area due to compression. Moreover, detrimental effects like intrabeam scattering or microbunching may increase the energy spread above the limit given by the preservation of the longitudinal emittance. All in all, the relative electron beam energy spread in x-ray FEL facilities can be as low as $10^{-5}$ or less.

The standard way to characterize the energy spread of the electron beam is from longitudinal phase-space (LPS, energy, and time) measurements. The electron beam is streaked in one transverse direction and measured with a two-dimensional profile monitor placed in a location with transverse dispersion in the opposite plane of the streaking. The streaking is normally achieved with an rf transverse deflector (TD). LPS measurements are typically done at electron beam energies of ≈100 MeV or higher to avoid space-charge effects. The energy spread can be obtained from the time resolved or *slice* beam size $\sigma_x$ as $\sigma_E = (E/\eta)\sigma_x$, where $E$ is the electron beam energy and $\eta$ is the transverse dispersion at the profile monitor. The resolution of this approach is limited by effects like the natural size of the electron beam and the resolution of the profile monitor. Recent work has suggested improving the resolution of the standard measurements by measuring the energy spread for different values of certain parameters such as the electron beam energy [20,21], the dispersion [22], or the transport lattice [23]. The TD induces a certain energy spread to the electron beam [24], which can be assessed by measuring the energy spread for different TD voltages [20–23,25].

These recent high-resolution measurements at rf photoinjectors have reported energy spread values much larger than anticipated by standard numerical simulations [20–23]. In particular, in [21], some of us showed that the energy spread increase is caused by intrabeam scattering and microbunching, effects not covered in standard modeling tools. These advances underline the importance of measuring the energy spread with high resolution and developing models to properly simulate effects like intrabeam scattering and microbunching.

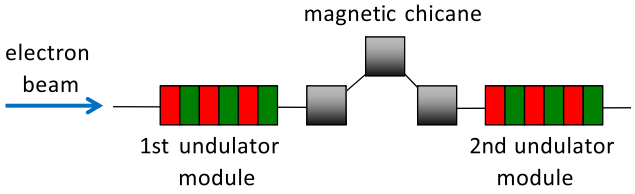


FIG. 1. Optical klystron layout. Image taken from [31].

As an alternative to direct LPS measurements, some methods have been proposed to estimate the energy spread of the electron beam from undulator radiation measurements, namely by using optical replicas [26], via coherent harmonic generation [27], or exploiting the optical klystron effect [28–34].

The work presented here deals with measuring the energy spread using the optical klystron mechanism. In its simplest version, the scheme includes two undulator modules and one magnetic chicane in between, as shown in Fig. 1. In the optical klystron configuration, the longitudinal dispersion of the chicane speeds up the FEL process and results in an increase of the radiation power produced in the undulators. With an induced correlated energy spread (energy modulation) in the first module, the optical klystron can convert this thanks to runtime differences into a current modulation, thus enhancing the bunching factor in the second module and with that the coherent emission. The performance is determined by the Landau damping effect of the energy spread. Thus, the relative energy spread of the beam can be obtained by measuring the radiation power as a function of the longitudinal dispersion of the chicane. Besides the undulator modules and the chicane, the approach requires a monitor to measure the radiation power or energy. This does not need to be an absolute measurement, so can be done, for instance, with a photodiode.

The optical klystron approach has some advantages with respect to the standard LPS measurement. Most importantly, the measurement resolution can be higher with the optical klystron. The standard LPS approach has difficulties reaching relative resolutions of $10^{-5}$ (equivalent to ≈1 keV before compression or ≈100 keV at the undulator), and cannot reach resolutions of $10^{-6}$ or below using standard components, while the optical klystron can potentially achieve this. We note, however, that in case of very low energy spread values, the induced energy spread in the undulator module before the chicane can be comparable or larger than the initial energy spread, thus falsifying the identification of the observed value as the initial energy spread. Another effect that can influence the measurement,

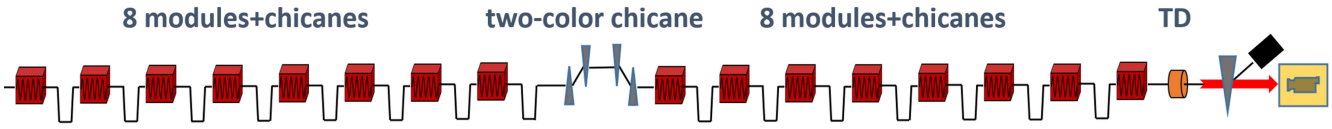


FIG. 2. Sketch of the Athos FEL beamline. See text for more details.

especially for relatively high electron beam energies (GeV level and higher), is quantum diffusion in the undulators [35,36]. We estimate this effect to be around 20 keV or less in our case (at a central beam energy of 3.4 GeV), which is insignificant for the measured values that we will show later. Another advantage of the optical klystron approach is that the measurement procedure is much simpler: it only requires a measurement of the radiation power as a function of the chicane strength, while the LPS-based measurement needs complicated and expensive time-resolved diagnostics, special care of beam optics, and performing measurements as a function of different parameters for an improved resolution. Finally, the optical klystron setup can be more cost-effective than the TD approach. Nevertheless, TDs are in some ways a standard diagnostics of the bunch duration, typically available at different locations of an x-ray FEL facility. An advantage of the TD approach is that it allows for a time-resolved measurement of the energy spread, while the optical klystron provides a single value averaged over the lasing part of the bunch. Another potential limitation of the optical klystron method is that it may provide unreliable results in the presence of microbunching instabilities [29].

The optical klystron method has been proposed and experimentally employed to derive the energy spread of the electron beam [28–34]. A notable example is Ref. [32], where the approach was used to estimate a relative energy spread of $3 \times 10^{-5}$. However, to the best of our knowledge, the method has never been experimentally validated against standard LPS measurements nor has its behavior been verified for different undulator configurations or compression scenarios. Here, we use the optical klystron approach to characterize the energy spread of the electron beam in a systematic way. First, we benchmark the approach with the standard TD method. Second, we verify, also with the help of the TD, that the reconstructed energy spread scales adequately with the electron beam duration according to the assumption that the longitudinal emittance is preserved. Third, we confirm that the reconstructed energy spread is consistent for different radiation wavelengths $\lambda$ and different undulator configurations. Our work demonstrates experimentally that the optical klystron mechanism represents a precise and high-resolution method to measure the energy spread of electron beams.

## II. MEASUREMENT SETUP AND PROCEDURE

The measurements were carried out at Athos [37], the soft x-ray FEL beamline of SwissFEL [38]. Figure 2 shows a sketch of Athos. The Athos undulator consists of 16 APPLE-X [39,40] modules capable of delivering variable magnetic field strength and polarization. The modules are interleaved with compact magnetic chicanes of 0.2 m each. The chicanes consist of four dipole magnets and can delay the electron beam by up to about 7 fs, corresponding to a maximum longitudinal dispersion of 4.2 μm (the longitudinal dispersion is about twice the delay, when the delay is expressed in units of length). In the middle of the undulator, there is an additional longer chicane (two-color chicane), not employed in this work, used to set larger delays up to 500 fs for two-color FEL operation [41].

### A. Optical-klystron-based measurement of the electron beam energy spread

The efficiency of the optical klystron mechanism strongly depends on the energy spread of the electron beam. In fact, the energy spread can be derived by measuring the radiation power or energy as a function of the longitudinal dispersion $R_{56}$ of the chicane. According to early literature, the relative energy spread of the beam $\sigma_\delta = \sigma_E/E$ can be obtained from the optimum longitudinal dispersion $R^*_{56}$, giving maximum radiation power, as (see, e.g., Ref. [28]):

$$\sigma_\delta = \frac{\lambda}{2\pi R^*_{56}}, \tag{2}$$

where $\lambda$ is the wavelength of the produced radiation. As seen in the above equation, for relatively low energy spreads, relatively large $R_{56}$ values are required to find the maximum optical klystron gain and therefore the energy spread of the beam. In case of limited chicane strength, one can still decrease the radiation wavelength to find $R^*_{56}$.

A recent revision of the optical klystron theory [33] demonstrates that the above equation is only valid for very small values of $\Lambda = \sigma_\delta/\rho$, where $\rho$ is the FEL or Pierce parameter [42] and that it can significantly overestimate the energy spread for comparatively large $\Lambda$. Note that for $\Lambda > 1$, there is no FEL amplification. Reference [33] proposes alternative ways to precisely estimate the electron beam energy spread. Here, we choose to apply the following expression defining the power gain of the optical klystron:

$$G = \frac{1}{9} + \frac{1}{9}\exp(-D^2\Lambda^2)[4 + 2\sqrt{3}D + D^2 - 13D^2\Lambda^2 - 2\sqrt{3}D^3\Lambda^2 + 7D^4\Lambda^4], \tag{3}$$

where $D = (2\pi R_{56}\rho)/\lambda$. When $\Lambda \ll D$, the maximum optical klystron gain is achieved for $D\Lambda = 1$, which corresponds to Eq. (2).

We reconstruct the energy spread of the electron beam by measuring the FEL pulse energy as a function of the $R_{56}$ of the chicanes and fitting the data with the above equation. Equation (3) is accurate for values of $\Lambda$ up to $\approx$0.1–0.2 [33], a condition that we estimate to be fulfilled for our parameters. As will be shown later, the maximum reconstructed relative energy spread of the electron beam is about $5 \times 10^{-4}$. For these conditions, we estimate [43] a Pierce parameter of at least $3 \times 10^{-3}$, corresponding to $\Lambda$ values of 0.17 or less. In our case, the results obtained from both equations are very similar: Eq. (2) slightly overestimates the energy spread by 5% or less with respect to the more precise Eq. (3).

The pulse energy measurement is accomplished with a photon gas detector [44] located after the undulator. Such devices require a minimum level of detectable pulse energy, in our case about one microjoule. Because of this, we use three to five undulator modules (depending on the photon energy and polarization) and scan simultaneously the chicanes in between to obtain a meaningful scan. Performing the measurement with more modules and chicanes is as valid as with two modules and one chicane, provided that there is no significant increase in the energy spread within the employed modules, which is the case in the measurements shown here. In general, one could use a photodiode as a radiation intensity monitor, which can measure significantly lower pulse energies than a gas detector, in case of having only two modules and one chicane.

### B. Standard measurement of the electron beam energy spread

The LPS measurements are performed after the undulator with an $X$-band rf TD [45]. The beam is streaked with the TD in the horizontal direction and the dispersion is in the vertical plane. The time calibration $C$ between the transverse coordinate on the screen and the time coordinate within the electron beam are obtained by measuring the central position of the electron beam in the streaking direction as a function of the TD phase (see, e.g., Ref. [46]). We obtain the electron beam rms duration from the transverse electron beam size at the two zero crossings of the TD. The beam size is determined by fitting a Gaussian fit to the transverse distribution of the electron beam. We consider that the measured energy spread $\sigma_{E,m}$ has two contributions: the true energy spread $\sigma_E$ and the energy spread induced by the TD $\sigma_{E,T}$. The latter can be expressed as [24]:

$$\sigma_{E,T} = ek_T V \cos(\phi)\sigma_T, \tag{4}$$

where $e$ is the elementary charge, $k_T$ is the rf wave number, $V$ is the integrated deflecting voltage, $\phi$ is the TD rf phase (the TD operates normally at the zero crossing such that $\cos(\phi) \approx 1$), and $\sigma_T$ is the average transverse beam size in the streaking direction at the TD location. Since the two contributions of the measured energy spread are independent, we can write

$$\sigma_{E,m}^2 = \sigma_E^2 + \sigma_{E,T}^2 = \sigma_E^2 + (ek_T\sigma_T)^2 V^2. \tag{5}$$

We determine the true energy spread by measuring the energy spread for different voltages $V$ and fitting the results with the above equation. These measurements are done for one zero crossing of the TD. In each case, the time calibration $C$ is only measured for the highest TD voltage. The TD voltages for which the time calibrations were measured are estimated as

$$V_c = \frac{CE}{ecR_{12}k_T}, \tag{6}$$

where $R_{12}$ is the transport matrix element relating a horizontal kick angle in the TD to a horizontal offset at the profile monitor, which is obtained from the lattice optics. The rest of the TD voltages are obtained by scaling $V_c$ assuming that the bunch duration stays the same. The estimated voltages are 10%–35% lower than the values set in the rf system due to power loss in the system, which is still under commissioning. We use the estimated voltages for the results presented here, noting that using the set voltages instead of the estimated voltages would change the reconstructed energy spread results shown later by only 2% or less.

Further potential contributions may affect the measured beam size in the dispersive direction and therefore the reconstructed energy spread, specifically contributions due to the natural electron beam size at the dispersive plane or the profile monitor resolution. In our case, the measured average slice beam sizes are above 130 μm, while the screen resolution is estimated to be better than 25 μm, and the expected natural beam size from the set optics should be less than this (the electron beam was matched before the TD). Consequently, we expect contributions from these two effects below a few percent. If these effects were significant, one could perform measurements not only as a function of the TD voltage but also as a function of some other parameter like the electron beam energy or the transverse dispersion, as realized in [20–22]. Moreover, in the presence of a significant energy chirp within the slices, there can be an artificial increase in the slice beam size resulting in an overestimation of the reconstructed energy spread. As we will see later, we estimate this effect to be insignificant in our case.

## III. MEASUREMENT RESULTS

We report here the results obtained during two measurement shifts. In the first shift, we measured the energy spread using the optical klystron effect for two different

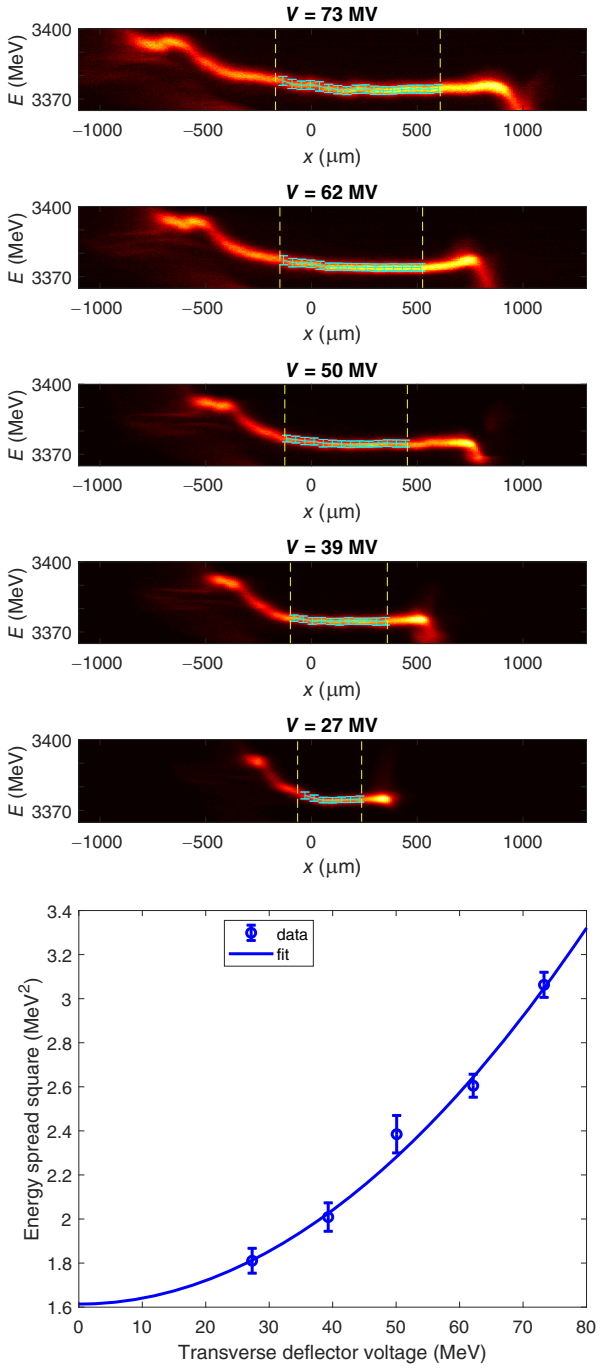


FIG. 3. Measurement example with the TD standard method. Top: single-shot images for different TD voltages. The dashed yellow lines define the region of interest for which the energy spread is calculated. The lines in these regions indicate the slice energy (points) and energy spread (error bars). Bottom: calculated energy spread as a function of the TD voltage. See text for more details.

radiation wavelengths (1.24 and 3.10 nm) and, for each of them, for helical and planar undulator configurations (corresponding to circular and linear horizontal polarization). The different wavelengths and polarizations were achieved by changing the undulator parameters. The electron bunch duration was measured to be 24 fs rms for all different undulator configurations. We benchmarked the results with the LPS using the TD. The TD measurement was done at the beginning and at the end of the shift. In the second shift, we used the optical klystron to reconstruct the energy spread for five different electron bunch durations (rms values from about 25 to 60 fs), which were obtained by varying the compression in the second part of the linac. The radiation wavelength was fixed at 2.36 nm and the undulator was set to helical configuration for all cases. We validated the results for one of the bunch durations with the standard TD approach. The transverse dispersion at the profile monitor was 0.345 m in the first shift and 0.296 m in the second shift. In both shifts, the electron bunch charge was 200 pC and the electron beam energy was around 3.4 GeV, as in standard operation. All error bars shown in the following correspond to statistical uncertainties of the reported measurements.

The results are shown in Figs. 3–5 and Table I. The results of one of the standard measurements based on LPS, the second one of the first shift, are shown in Fig. 3. The figure shows single-shot images for different voltages and the calculated energy spread as a function of the TD voltage. The horizontal axis of the images is the direct horizontal position, proportional to time, but has not been converted to time for better visualization of the different streaking amplitudes as a function of voltage. The vertical axis has been converted to energy based on the dispersion. We took ten measurement shots at every voltage. The time calibration was measured for the largest voltage of around 70 MV to be $38.0 \pm 3.0$ μm/fs, giving an rms bunch duration of around 24 fs. At each voltage, we calculate the energy spread as the average of the slice-energy spread at the core of the bunch, averaged over the different shots. We observe in Fig. 3 that the core part of the bunch has a rather flat energy profile, which is achieved through wakefields in the accelerator beamline. Consequently, we do not expect any artificial increase of the slice beam size (and therefore in the energy spread) due to an energy chirp within the slices. In the example of Fig. 3, the true energy spread of the beam, obtained by fitting the data with Eq. (5), is $1.27 \pm 0.02$ MeV. The other TD measurement, performed at the beginning of the first shift, resulted in an energy spread of $1.19 \pm 0.12$ MeV, in good agreement with the measurement at the end of the shift. During the second shift, a TD measurement was only done at the shortest bunch duration and gave a reconstructed energy spread of $1.62 \pm 0.13$ MeV.

Figure 4 displays the optical klystron scans for both shifts. The top plot of the figure shows the four scans executed during the first shift for two different radiation wavelengths and two different undulator configurations (helical and planar) for the same compression setting. The four measurements result in an equivalent energy spread of

TABLE I. Measured rms bunch durations and energy spread for the different cases.

| Shift | Pulse duration (fs) | Radiation wavelength/ undulator configuration | Energy spread from optical klystron (MeV) | Energy spread from TD (MeV) |
|---|---|---|---|---|
| 1 | $23.7 \pm 0.9$ | 1.24 nm/helical | $1.10 \pm 0.09$ | $1.19 \pm 0.12$ |
| | (beginning) | 1.24 nm/planar | $1.21 \pm 0.09$ | (beginning) |
| | $23.9 \pm 1.0$ | 3.10 nm/helical | $1.18 \pm 0.06$ | $1.27 \pm 0.02$ |
| | (end) | 3.10 nm/planar | $1.22 \pm 0.09$ | (end) |
| 2 | $25.4 \pm 2.6$ | 2.36 nm/helical | $1.67 \pm 0.02$ | $1.62 \pm 0.13$ |
| | $31.0 \pm 3.9$ | 2.36 nm/helical | $1.13 \pm 0.05$ | |
| | $37.9 \pm 2.9$ | 2.36 nm/helical | $1.04 \pm 0.05$ | |
| | $55.8 \pm 2.6$ | 2.36 nm/helical | $0.76 \pm 0.05$ | |
| | $62.0 \pm 4.3$ | 2.36 nm/helical | $0.69 \pm 0.04$ | |

around 1.2 MeV. This value is consistent with the energy spread obtained from the TD measurements (see detailed numbers in Table I): equivalent to the measurement performed at the beginning of the shift, several percent lower than the result of the measurement at the end of the shift.

The bottom plot of Fig. 4 shows the optical klystron scans for different electron bunch durations, performed in the second shift. The radiation wavelength was fixed at 2.36 nm, and the undulator was set to helical configuration for all cases. The estimated energy spread as a function of the beam duration is shown in Fig. 5 and Table I. The TD measurement obtained at the shortest beam duration fits well with the optical-klystron-based measurement. Figure 5 displays a fit of the type $A/\sigma_t$, where $\sigma_t$ are the bunch durations and $A$ is a fit parameter corresponding to the longitudinal emittance in terms of pulse duration and energy spread. We assume here that the different compression configurations do not change the longitudinal emittance or, in other words, that no effects such as microbunching instability or intrabeam scattering are significant in the second part of the linac where the compression is changed. We reconstruct $A = 41.4 \pm 1.7$ MeV fs. As can be seen from the figure, the fit covers all measured points reasonably well.

The $A$ parameter of the first measurement shift was significantly lower (around 28 MeV fs using the energy spread obtained with the optical klystron) than in the second shift (41.4 MeV fs). This could be due to different contributions of effects such as intrabeam scattering or microbunching in the injector or in the linac between the 2 days, possibly related to different injector or compression settings. According to [21] the longitudinal emittance in the injector area is currently at best around 27 MeV fs: the energy spread for standard optics and 200 pC bunch charges can be 7 keV, and the rms bunch duration is 3.8 ps for this beam charge. During the first measurement shift, the best longitudinal emittance could be obtained and preserved until the Athos undulator, while for the second

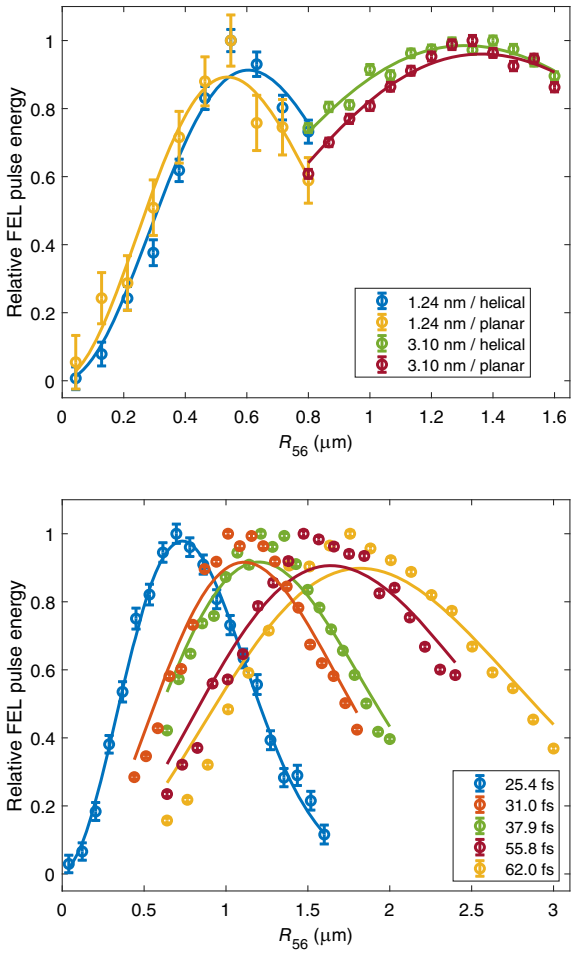


FIG. 4. Optical klystron scans. Top: measurement for two radiation wavelengths (1.24 and 3.1 nm) and two different undulator configurations (helical and planar) for an electron bunch duration of 24 fs. Bottom: measurement for different electron beam durations for a radiation wavelength of 2.36 nm and helical undulator configuration. The dots indicate measured values and the lines correspond to fits obtained from Eq. (3).

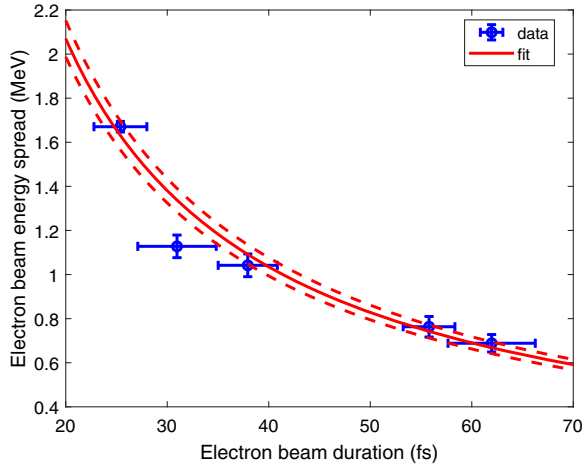


FIG. 5. Reconstructed energy spread using the optical klystron effect as a function of the measured electron bunch duration. The blue points correspond to measured values. The red lines illustrate the fit: central value (solid line) and standard deviation (dashed lines). See text for more details.

shift, the longitudinal emittance was degraded by about 50%, either in the injector or later in the linac.

## IV. CONCLUSION

To conclude, we have established the optical klystron effect as a precise and high-resolution approach to reconstruct the energy spread of high-brightness electron beams. We have benchmarked the method with the standard approach of measuring the LPS of the electron beam with a TD. We have also verified the consistency of the measurements as a function of different electron beam durations and radiation parameters (wavelength and polarization). The results validate the measurement based on the optical klystron, which can be relevant where TDs are not available or to reconstruct low energy spread values, where the conventional approach may be resolution limited, such as in ultra high-brightness electron beam sources.

## ACKNOWLEDGMENTS

We thank all the technical groups involved in the operation of SwissFEL.

[1] Z. Huang and K.-J. Kim, Phys. Rev. ST Accel. Beams **10**, 034801 (2007).
[2] B. W. J. McNeil and N. R. Thompson, Nat. Photonics **4**, 814 (2010).
[3] C. Pellegrini, A. Marinelli, and S. Reiche, Rev. Mod. Phys. **88**, 015006 (2016).
[4] J. B. Hastings, F. M. Rudakov, D. H. Dowell, J. F. Schmerge, J. D. Cardoza, J. M. Castro, S. M. Gierman, H. Loos, and P. M. Weber, Appl. Phys. Lett. **89**, 184109 (2006).
[5] P. Musumeci, J. Moody, and C. Scoby, Ultramicroscopy **108**, 1450 (2008).
[6] S. Boucher, P. Frigola, A. Murokh, M. Ruelas, I. Jovanovic, J. Rosenzweig, and G. Travish, Nucl. Instrum. Methods Phys. Res., Sect. A **608**, S54 (2009).
[7] W. Graves, W. Brown, F. Kaertner, and D. Moncton, Nucl. Instrum. Methods Phys. Res., Sect. A **608**, S103 (2009).
[8] J. S. Fraser, R. L. Sheffield, E. R. Gray, and G. W. Rodenz, IEEE Trans. Nucl. Sci. **32**, 1791 (1985).
[9] C. Hernandez-Garcia, P. G. O'Shea, and M. L. Stutzman, Phys. Today **61**, No. 2, 44 (2008).
[10] M. Schaer, A. Citterio, P. Craievich, S. Reiche, L. Stingelin, and R. Zennaro, Phys. Rev. Accel. Beams **19**, 072001 (2016).
[11] B. E. Carlsten, P. M. Anisimov, C. W. Barnes, Q. R. Marksteiner, R. R. Robles, and N. Yampolsky, Instruments **3**, 52 (2019).
[12] R. R. Robles, O. Camacho, A. Fukasawa, N. Majernik, and J. B. Rosenzweig, Phys. Rev. Accel. Beams **24**, 063401 (2021).
[13] T. G. Lucas, H.-H. Braun, P. Craievich, R. Fortunati, N. Kirchgeorg, A. Magazinik, M. Pedrozzi, J.-Y. Raguin, S. Reiche, M. Schaer *et al.*, Phys. Rev. Accel. Beams **26**, 103401 (2023).
[14] A. R. Maier, A. Meseck, S. Reiche, C. B. Schroeder, T. Seggebrock, and F. Grüner, Phys. Rev. X **2**, 031019 (2012).
[15] T. André, I. A. Andriyash, A. Loulergue, M. Labat, E. Roussel, A. Ghaith, M. Khojoyan, C. Thaury, M. Valléau, F. Briquez *et al.*, Nat. Commun. **9**, 1334 (2018).
[16] A. Deng, O. S. Karger, T. Heinemann, A. Knetsch, P. Scherkl, G. G. Manahan, A. Beaton, D. Ullmann, G. Wittig, A. F. Habib *et al.*, Nat. Phys. **15**, 1156 (2019).
[17] S. Di Mitri, Photonics **2**, 317 (2015).
[18] E. Allaria, D. Castronovo, P. Cinquegrana, P. Craievich, M. D. Forno, M. B. Danailov, G. D'Auria, A. Demidovich, G. D. Ninno, S. D. Mitri *et al.*, Nat. Photonics **7**, 913 (2013).
[19] P. R. Ribič, A. Abrami, L. Badano, M. Bossi, H.-H. Braun, N. Bruchon, F. Capotondi, D. Castronovo, M. Cautero, P. Cinquegrana *et al.*, Nat. Photonics **13**, 555 (2019).
[20] E. Prat, P. Dijkstal, E. Ferrari, A. Malyzhenkov, and S. Reiche, Phys. Rev. Accel. Beams **23**, 090701 (2020).
[21] E. Prat, P. Craievich, P. Dijkstal, S. D. Mitri, E. Ferrari, T. G. Lucas, A. Malyzhenkov, G. Perosa, S. Reiche, and T. Schietinger, Phys. Rev. Accel. Beams **25**, 104401 (2022).
[22] S. Tomin, I. Zagorodnov, W. Decking, N. Golubeva, and M. Scholz, Phys. Rev. Accel. Beams **24**, 064201 (2021).
[23] H. Qian, M. Krasilnikov, A. Lueangaramwong, X. Li, O. Lishilin, Z. Aboulbanine, G. Adhikari, N. Aftab, P. Boonpornprasert, G. Georgiev *et al.*, Phys. Rev. Accel. Beams **25**, 083401 (2022).
[24] K. Floettmann and V. V. Paramonov, Phys. Rev. ST Accel. Beams **17**, 024001 (2014).
[25] D. Ratner, C. Behrens, Y. Ding, Z. Huang, A. Marinelli, T. Maxwell, and F. Zhou, Phys. Rev. ST Accel. Beams **18**, 030704 (2015).
[26] E. Saldin, E. Schneidmiller, and M. Yurkov, Nucl. Instrum. Methods Phys. Res., Sect. A **539**, 499 (2005).
[27] C. Feng, T. Zhang, J. Chen, H. Deng, M. Zhang, X. Wang, B. Liu, T. Lan, D. Wang, and Z. Zhao, Phys. Rev. ST Accel. Beams **14**, 090701 (2011).

[28] Y. Ding, P. Emma, Z. Huang, and V. Kumar, Phys. Rev. ST Accel. Beams **9**, 070702 (2006).
[29] G. Penco, E. Allaria, G. D. Ninno, E. Ferrari, and L. Giannessi, Phys. Rev. Lett. **114**, 013901 (2015).
[30] G. Penco, E. Allaria, G. D. Ninno, E. Ferrari, L. Giannessi, E. Roussel, and S. Spampinati, Photonics **4**, 15 (2017).
[31] E. Prat, E. Ferrari, S. Reiche, and T. Schietinger, Phys. Rev. Accel. Beams **20**, 040702 (2017).
[32] G. Penco, G. Perosa, E. Allaria, S. Di Mitri, E. Ferrari, L. Giannessi, S. Spampinati, C. Spezzani, and M. Veronese, Phys. Rev. Accel. Beams **23**, 120704 (2020).
[33] G. Geloni, M. Guetg, S. Serkez, and E. Schneidmiller, Phys. Rev. Accel. Beams **24**, 090702 (2021).
[34] E. Prat, E. Ferrari, M. Calvi, R. Ganter, S. Reiche, and T. Schmidt, Appl. Phys. Lett. **119**, 151102 (2021).
[35] E. Saldin, E. Schneidmiller, and M. Yurkov, Nucl. Instrum. Methods Phys. Res., Sect. A **381**, 545 (1996).
[36] S. Tomin, E. Schneidmiller, and W. Decking, Sci. Rep. **13**, 1605 (2023).
[37] E. Prat, A. A. Haddad, C. Arrell, S. Augustin, M. Boll, C. Bostedt, M. Calvi, A. L. Cavalieri, P. Craievich, A. Dax *et al.*, Nat. Commun. **14**, 5069 (2023).
[38] E. Prat, R. Abela, M. Aiba, A. Alarcon, J. Alex, Y. Arbelo, C. Arrell, V. Arsov, C. Bacellar, C. Beard *et al.*, Nat. Photonics **14**, 748 (2020).
[39] M. Calvi, C. Camenzuli, E. Prat, and T. Schmidt, J. Synchrotron Radiat. **24**, 600 (2017).
[40] T. Schmidt and M. Calvi, Synchrotron Radiat. News **31**, 35 (2018).
[41] E. Prat, P. Dijkstal, E. Ferrari, R. Ganter, P. Juranič, A. Malyzhenkov, S. Reiche, T. Schietinger, G. Wang, A. A. Haddad *et al.*, Phys. Rev. Res. **4**, L022025 (2022).
[42] R. Bonifacio, C. Pellegrini, and L. M. Narducci, Opt. Commun. **50**, 373 (1984).
[43] M. Xie, in *Proceedings of the 1995 Particle Accelerator Conference, Dallas, TX, 1995* (IEEE, New York, 1996), p. 183.
[44] A. A. Sorokin, Y. Bican, S. Bonfigt, M. Brachmanski, M. Braune, U. F. Jastrow, A. Gottwald, H. Kaser, M. Richter, and K. Tiedtke, J. Synchrotron Radiat. **26**, 1092 (2019).
[45] P. Craievich, Z. Geng, F. Marcellini, C. Kittel, S. Reiche, T. Schietinger, G. Wang, and E. Prat, in *X-Ray Free-Electron Lasers: Advances in Source Development and Instrumentation VI*, edited by T. Tschentscher, L. Patthey, M. Zangrando, and K. Tiedtke, SPIE Proceedings Vol. 11038 (SPIE-International Society for Optical Engineering, Bellingham, WA, 2023).
[46] E. Prat, A. Malyzhenkov, and P. Craievich, Rev. Sci. Instrum. **94**, 043103 (2023).